Minerals **2012**, *2*, 365-384; doi:10.3390/min2040365

OPEN ACCESS

minerals

ISSN 2075-163X
www.mdpi.com/journal/minerals

Article

Platinum-Group Minerals in Chromitites of the Niquelândia Layered Intrusion (Central Goias, Brazil): Their Magmatic Origin and Low-Temperature Reworking during Serpentinization and Lateritic Weathering

Giorgio Garuti [1,*], Federica Zaccarini [1], Joaquin A. Proenza [2], Oskar A. R. Thalhammer [1] and Nelson Angeli [3]

[1] Department of Applied Geosciences and Geophysics, Montan Universität Leoben, Leoben 8700, Austria; E-Mails: federica.zaccarini@unileoben.ac.at (F.Z.); oskar.thalhammer@unileoben.ac.at (O.A.R.T.)

[2] Departament of Crystallography, Mineralogy and Ore Deposits, Faculty of Geology, Universitat de Barcelona, Barcelona 08028, Spain; E-Mail: japroenza@ub.edu

[3] Departament of Petrology and Metallogeny, Universidade Estadual Paulista, Rio Claro 13500, SP, Brazil; E-Mail: nangeli@rc.unesp.br

***** Author to whom correspondence should be addressed; E-Mail: giorgio.garuti@unileoben.ac.at; Tel.: +43-3842-402-6218; Fax: +43-3842-402-6202.

Received: 3 September 2012; in revised form: 19 October 2012 / Accepted: 19 October 2012 / Published: 30 October 2012

Abstract: A variety of platinum-group-minerals (PGM) have been found to occur associated with the chromitite and dunite layers in the Niquelândia igneous complex. Two genetically distinct populations of PGM have been identified corresponding to phases crystallized at high temperatures (primary), and others formed or modified during post-magmatic serpentinization and lateritic weathering (secondary). Primary PGM have been found in moderately serpentinized chromitite and dunite, usually included in fresh chromite grains or partially oxidized interstitial sulfides. Due to topographically controlled lateritic weathering, the silicate rocks are totally transformed to a smectite-kaolinite-garnierite-amorphous silica assemblage, while the chromite is changed into a massive aggregate of a spinel phase having low-Mg and a low Fe^{3+}/Fe^{2+} ratio, intimately associated with Ti-minerals, amorphous Fe-hydroxides, goethite, hematite and magnetite. The PGM in part survive alteration, and in part are corroded as a result of deep chemical weathering. Laurite is altered to Ru-oxides or re-crystallizes together with secondary Mg-ilmenite. Other PGM,

especially the Pt-Fe alloys, re-precipitate within the altered chromite together with kaolinite and Fe-hydroxides. Textural evidence suggests that re-deposition of secondary PGM took place during chromite alteration, controlled by variation of the redox conditions on a microscopic scale.

Keywords: Chromitite; PGM; laterite; weathering; Niquelândia

1. Introduction

The Niquelândia igneous complex, exposed in Central Goias (Figure 1A), was recognized as a layered intrusion [1]. According to geochemical and geochronological data, the complex was emplaced in the Middle Proterozoic (1560–1600 Ma) as a result of continental rifting and underwent amphibolite to granulite facies metamorphism at about 770–795 Ma [2,3]. Final convergence and continental collision caused deformation and disruption at about 630 Ma [4]. During Lower-Tertiary erosion, corresponding to the *Sul-Americano* cycle, ultramafic units in the lower part of the intrusion underwent supergene alteration and weathering originating in a thick laterite cover with silicate-Ni deposits [5].

The Niquelândia complex is similar to many other layered intrusions (*i.e.*, Bushveld, Stillwater, Great Dyke, Campo Formoso), and it contains chromite deposits (Figure 1B) with associated platinum-group element (PGE) geochemical anomalies [6]. A study of polished sections and heavy-mineral concentrates revealed that the majority of the PGE occur in specific platinum-group minerals (PGM) occurring as microscopic grains (<20 μm) unevenly disseminated in chromitites and their host rock [7–9]. As pointed out by [7], the chromitites contain two genetically distinct populations of PGM: The "primary" PGM, crystallized at high temperatures, and the "secondary" PGM, formed at relatively low temperatures, during post-magmatic evolution of the complex.

In this study, we summarize data from previous works, and present new results of a detailed investigation of the chromite-PGM paragenesis showing that the primary PGM were deposited at high temperature under relatively high sulfur fugacity, and that they underwent mineralogical reworking at low-temperature under variable redox conditions. This was a result of serpentinization (hydrothermal?) and weathering alteration (lateritization) of the ultramafic rocks under favorable morphologic and climatic conditions.

Figure 1. (**A**) Geographic location of the Niquelândia igneous complex; (**B**) Geological setting of the chromitite layers; BGZ = basal gabbro zone, BPZ + LUZ = basal peridotite zone and layered ultramafic zone, LGZ = lower gabbro zone, W − E = geologic profile in Figure 2 (Modified after [6]).

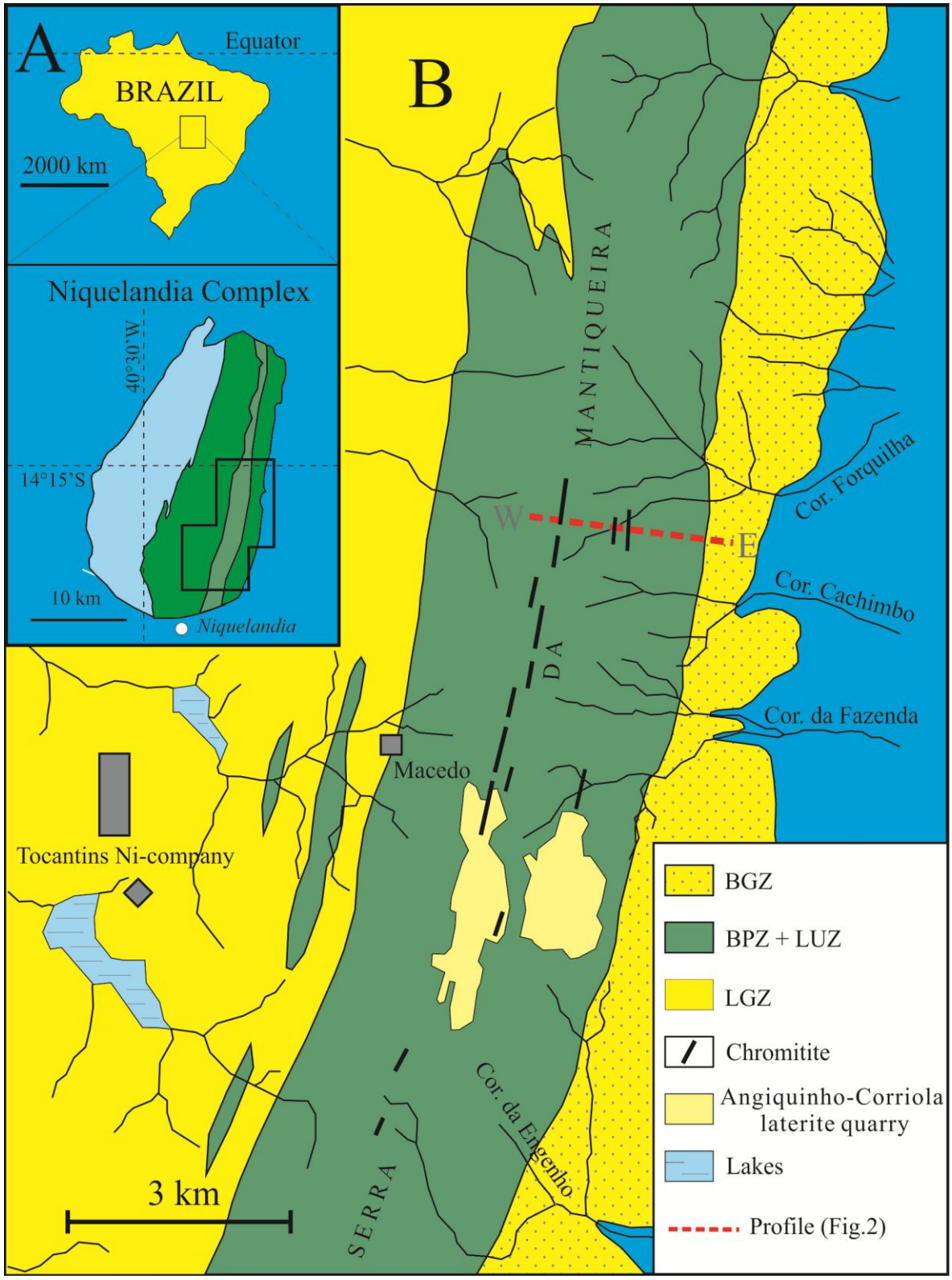

Figure 2. Geologic profile W – E showing stratigraphic location of the two chromitite horizons CHR-1 and CHR-2; Note that the upper chromitite CHR-2 occurs within the laterite cover in the highland of Serra da Mantiqueira. (Vertical and horizontal scale are in meters).

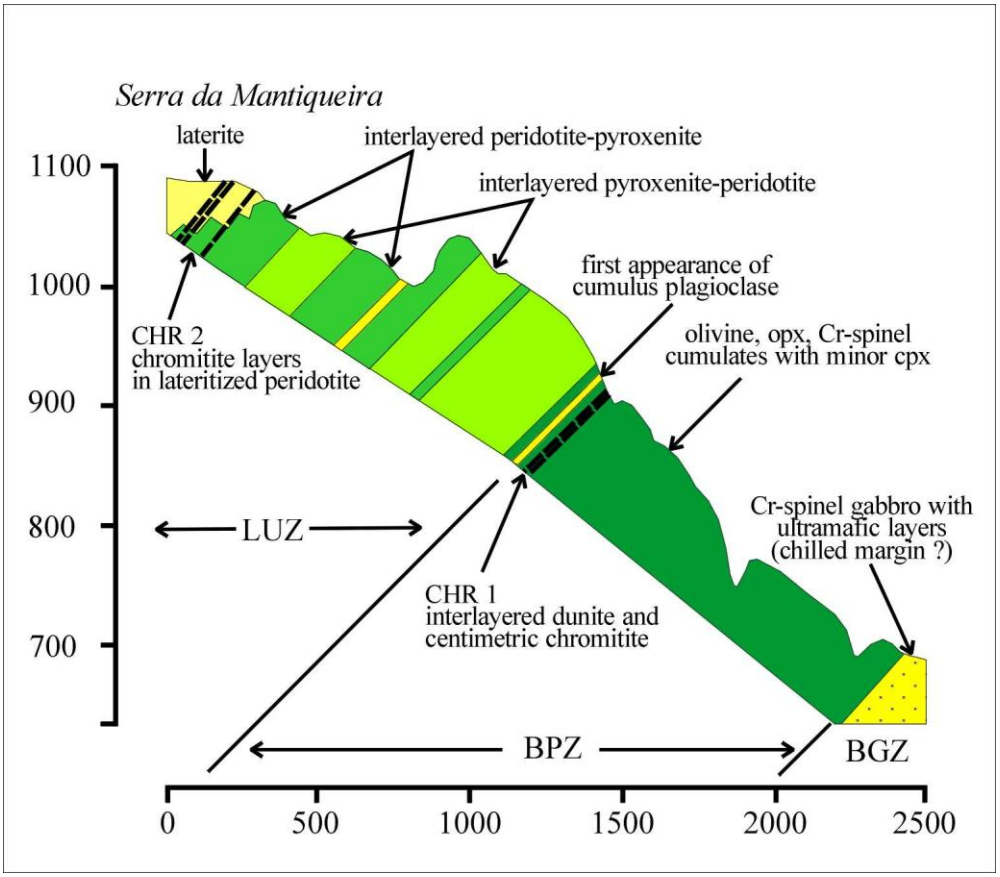

2. Analytical Techniques

This study is based on the investigation of 50 polished sections obtained from 16 chromitite samples and 6 host rocks, collected along a geologic profile cutting across the two major chromitite horizons in the ultramafic zone of the Niquelândia layered intrusion (Figure 2).

Electron microprobe analyses of chromite, silicates and PGM were performed using a Superprobe JEOL JXA 8200 instrument operated at the Eugen F. Stumpfl Laboratory of Leoben University (Austria). Back scattered electron (BSE) images of the PGM were obtained at the Leoben laboratory as well as at the Serveis Cientificotècnicos of Barcelona University.

Chromite and silicates were analyzed in WDS mode with an accelerating voltage of 15 kV and a beam current of 10 nA, using the Kα lines for Mg, Si, Ca, K, Al, F, Cl, Ti, V, Cr, Mn, Fe, Ni and Zn. Natural K-feldspar, albite, atacamite, diopside, chromite, rhodonite, ilmenite and metallic V, Ni and Zn were used as reference materials. The counting times for peak and background were 20 s and 10 s respectively. The amount of Fe^{3+} in the spinel was calculated assuming the ideal spinel stoichiometry, $R^{2+}O$ and $R^{3+}{}_2O_3$. X-ray Diffraction was used in the study of the laterite matrix of the CHR-2 chromitite.

The PGM and associated sulfides had been previously located by scanning polished sections using both reflected light (in air) and electron microscopes. They were quantitatively analyzed in the WDS mode, with an accelerating voltage of 20 kV and 10 nA beam current, allowing a beam diameter of about 1 μm or less. The counting times on peak and backgrounds were 15 s and 5 s respectively. The Kα lines were used for S, As, Fe, Cu and Ni; Lα for Rh, Pd, Pt, Sb and Te, and Mα for Hg. The reference materials were pure metals for the PGE, synthetic NiS, SbBi and Pd_3HgTe, natural chalcopyrite and niccolite for Ni, Hg, Fe, Cu, S, Te, Sb and As. The following diffracting crystals were selected: PETJ for S, Te; PETH for Ru, Os, Rh, Hg, Sb; LIF for Cu; LIFH for Ni, Ir, Pt; and TAP for As. Automatic corrections were performed for interferences involving Rh-Pd overlap. The detection limits (wt %) of the analyzed elements are: As = 0.40, S = 0.01, Sb = 0.05, Ni = 0.04, Fe = 0.02, Cu = 0.05, Os = 0.08, Ir = 0.1, Ru = 0.02, Rh = 0.01, Pt = 0.1, Pd = 0.02.

3. Geological Setting and Petrography of the Chromitites

Two major chromitite horizons have been documented so far in the ultramafic sequence of the Niquelândia layered intrusion [7]. They are located at about 1 km and 2 km from the base, respectively, being concordant with the N-S strike and the 30°–60° westwards dipping of the igneous stratigraphy (Figure 2). The two chromitite horizons display different styles of low-temperature alteration, apparently controlled by their topographic location in the landscape.

The lower horizon (CHR-1) is exposed along the eastern, steep slope of Serra da Mantiqueira, along the Corrego Forquilha. Here, lateritic weathering is absent, and the chromitite occurs as centimeter thick seams and schlieren within partly serpentinized peridotite composed of olivine and pyroxene relics in a matrix of lizardite, chrysotile, talc, chlorite and carbonates. The chromitite contains rare accessory sulfides accounting for 50–350 ppm total sulfur. The sulfides tend to increase in the adjacent dunite (400–1200 ppm sulfur) suggesting that sulfur saturation was achieved during this stage of fractionation [10]. The drop-like morphology of the interstitial sulfides is consistent with segregation of an intercumulus sulfide liquid, although their mineral assemblage, mainly composed of pentlandite veined with magnetite, appears to be a result of late alteration [10]. The calculated Ni/Fe distribution-coefficient between olivine and sulfide is in excess of 20 (Figure 3), indicating that the sulfide lost part of the Fe^{2+} by oxidation, probably during serpentinization of the ultramafic rocks [11].

The upper horizon (CHR-2) crops out in an almost flat area of the Serra da Mantiqueira highland. It embraces several disrupted layers of 5–30 cm, occasionally up to ~1 m thick, distributed over a stratigraphic interval of some hundred meters [6].

The layers are completely embedded in a laterite soil derived from weathering of the original ultramafic country rock, presumably dunite or harzburgite. The CHR-2 chromitite consists of a hard, completely massive aggregate of closely interlocked chromite grains, up to 3 cm in size. Silicates are extremely scarce, completely altered to smectite, kaolinite, rare serpentine and amorphous silica, usually intergrown with amorphous Fe-hydroxides, goethite, limonite, hematite, ferrian-chromite and magnetite. Abundant Mg-ilmenite and rutile occurs as rounded or ameboid grains aligned along grain-boundaries and cracks in altered chromite (Figure 4), suggesting splitting of Ti out of chromite during chemical weathering.

Figure 3. Relationships between the NiO/FeO ratio in olivine and the NiS/FeS ratio in the coexisting sulfides from the partially serpentinized dunite hosting CHR-1 chromitite layers. Lines of constant distribution-coefficient KD = 20 and KD = 40 are indicated. The NiS/FeS ratio in sulfide was calculated combining the modal proportion and microprobe composition of pentlandite, chalcopyrite, and pyrrhotite constituting the interstitial droplets in the dunite.

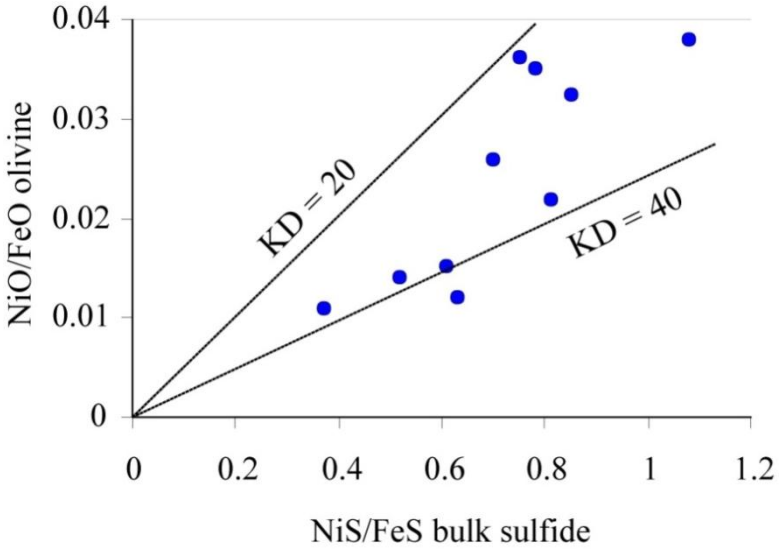

Figure 4. Vermicular aggregates of Mg-ilmenite and rutile, and kaolinite filled pores in CHR-2 massive chromitite. Parallel Nichols reflected light picture, long side = 1.0 mm.

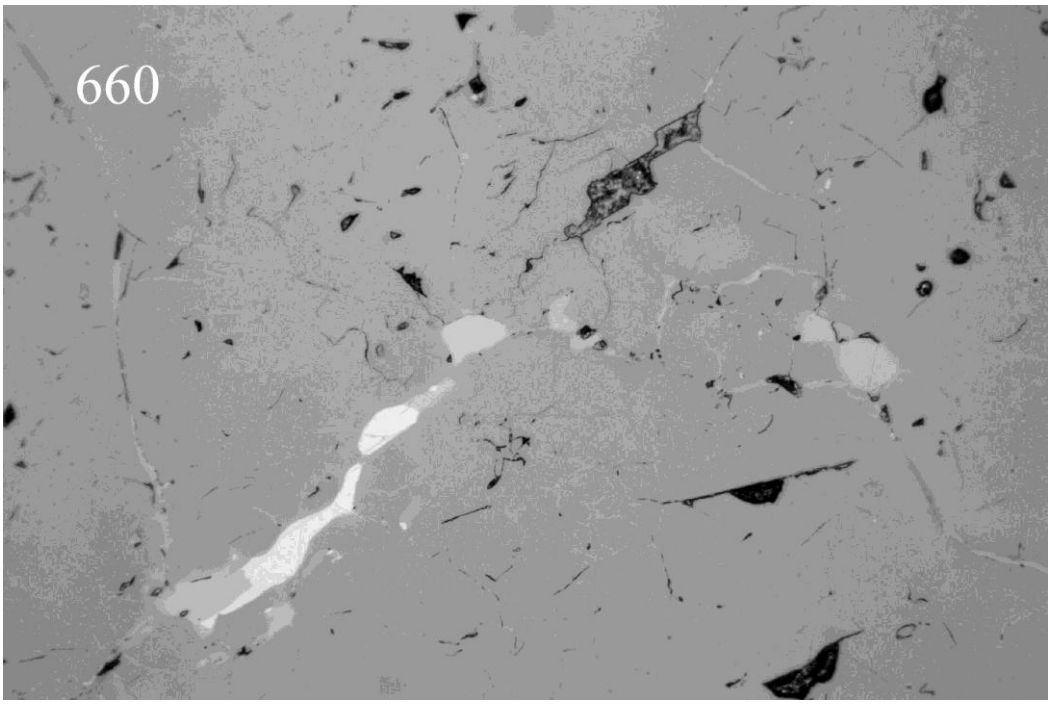

4. Chromite Alteration

Post-magmatic serpentinization and lateritic weathering have produced different types of alteration of the chromite.

Chromitites from the CHR-1 horizon are only slightly affected by serpentinization, showing limited alteration into ferrian-chromite along grain boundaries in contact with the serpentinized matrix. Alteration rims are more extensively developed in the accessory chromite in the dunite. The rims consist of spongy ferrian-chromite and chromian-magnetite locally intermixed with a fine grained chlorite (Figure 5). Chemical changes involve sharp decrease of Al_2O_3 and MgO in the alteration rims, accompanied by an increase in FeO and Fe_2O_3, while Cr_2O_3 is floating but showing a general decrease. Notably, the Fe_2O_3/FeO increases remarkably in the outermost alteration zone, indicating progressive oxidation.

Figure 5. Chemical variation across the chromitite core (fresh chromite) to rim (ferrian chromite) and boundary (chromian magnetite) zoning in accessory chromite from the serpentinized dunite host of the CHR-1 horizon.

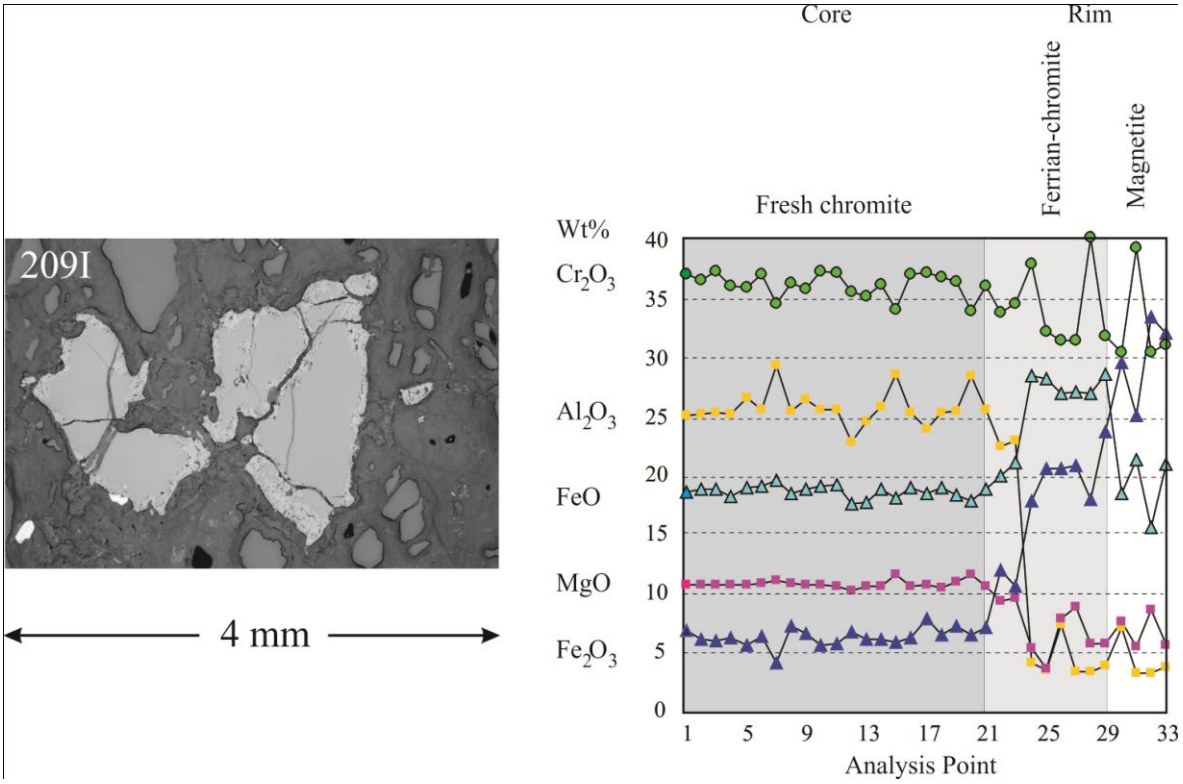

In the CHR-2 chromitites, chromite displays a complex zoning with a core composed of solid chromite, rimmed by a spinel phase densely pitted with pores (Figure 6). The pores are filled with secondary silicate minerals (mainly kaolinite and smectite). The alteration pattern involves depletion of MgO and Fe_2O_3 in the pitted chromite and a general increase of Al_2O_3 and FeO, resulting in a slight increase of the reflectivity (Figure 6). This alteration scheme showing a decrease of the Fe_2O_3/FeO ratio is contrary to that of the ferrian-chromite rims produced during serpentinization, and is ascribed to the different redox condition prevailing during lateritic weathering.

Figure 6. Chromite alteration patterns in laterite hosted chromitite CHR-2. The dark, solid chromite may represent the primary magmatic composition. The more reflective, pitted chromite is believed to be a result of the deep chemical weathering under lateritic conditions.

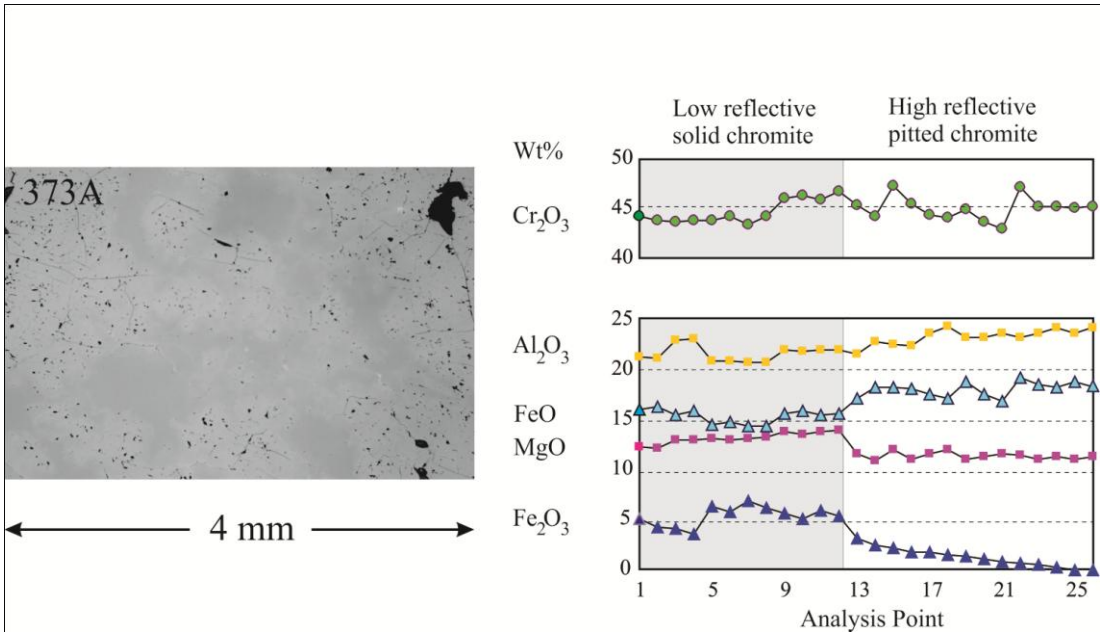

5. Mineralogy and Paragenesis of the Platinum-Group Minerals

A summary of the PGM recovered from the Niquelândia chromitite and dunite is given in Table 1, while Tables 2 and 3 provide a list of representative compositions obtained with an electron microprobe. The compositions of major PGM are presented in the relevant diagrams (Figure 7).

Table 1. Mineralogy and texture of Platinum-group minerals (PGM) in chromitites and associated dunite of the Niquelândia layered intrusion.

mineral	ideal formula	morphology	common association	host-phase	occurrence
laurite	$(Ru,Os,Ir)S_2$	euhedral-subhedral	pentladite-silicates	chromite-serpentine	CHR-1,CHR-2, dunite
erlichmanite	$(Os,Ru,Ir)S_2$	euhedral-subhedral	silicates	chromite	CHR-1,CHR-2
kashinite *	Ir_2S_3	subhedral	singlephase	chromite	CHR-2
iridosmine	Os-Ir	euhedral-subhedral	erlichmanite-singlephase	chromite	CHR-1,CHR-2
unnamed Ir-Ni sulfide	(Ir,Ni)-S	bleb	pentladite	chromite	CHR-1
undetermined Os-Ir sulfide	(Os,Ir)-S	bleb	pentladite	chromite	CHR-2
irarsite	IrAsS	subhedral	laurite-iridosmine	chromite	CHR-2
malanite	$Cu(Pt,Ir)_2S_4$	subhedral	singlephase	chromite	CHR-2
unnamed Ru-Fe oxide	Ru-O	rounded	laurite	Fe-chromite	CHR-2
isoferroplatino-type *	Pt_3Fe	anhedral (?)	Fe-hydroxide	Fe-chromite	CHR-2
tetraferroplatino type	Pt(Fe,Ni,Cu)	anhedral	kaolinite, Fe-hydroxide	Fe-chromite	CHR-1,CHR-2
tetraferroplatino-type	PtFe	rounded	singlephase	orthopyroxene	dunite
geversite	$Pt(Sb,Bi)_2$	euhedral	pentlandite-magnetite	interstitial sulfide bleb	dunite

Table 1. *Cont.*

mineral	ideal formula	morphology	common association	host-phase	occurrence
sudburyite	(Pd,Ni)Sb	euhedral	pentlandite-magnetite	interstitial sulfide bleb	dunite
sobolevskite	PdSb	euhedral	pentlandite-magnetite	interstitial sulfide bleb	dunite
kotulskite	Pd(Te,Bi)	euhedral	pentlandite-magnetite	interstitial sulfide bleb	dunite
moncheite	$PtTe_2$	anhedral	Fe-chromite	accessory chromite	dunite
stumpflite	Pt(Sb,Bi)	anhedral	Fe-chromite	accessory chromite	dunite

***** Found exclusively in HS-concentrates [9].

Table 2. Electron microprobe analyses of laurite and erlichmanite from Niquelândia.

Laurite	Os	Ir	Ru	Rh	Pt	Pd	Fe	Ni	Cu	S	As	total
55-3 *****	23.80	7.68	31.50	–	–	–	–	–	–	32.26	1.89	97.13
211C-1a *****	15.04	3.15	43.77	–	–	–	–	–	–	36.25	1.50	99.71
609A-16*****	20.68	5.29	32.42	1.39	–	1.85	1.07	0.08	0.01	35.59	1.42	99.80
615A-2 *****	7.40	3.70	51.70	–	0.08	–	–	0.15	–	36.20	–	99.23
615F-6*****	13.18	6.03	40.53	0.83	–	2.03	1.48	0.19	0.12	34.69	1.68	100.76
373A-2	30.29	14.19	21.21	2.05	–	–	–	0.15	–	29.96	0.39	98.24
453A-1	31.38	6.80	28.20	–	–	–	–	0.17	–	31.26	1.17	98.98
454-5	24.00	5.50	32.90	0.29	–	1.30	1.10	0.16	–	33.70	0.74	99.69
454-9a	31.10	6.40	20.10	1.80	–	–	5.31	–	–	33.50	1.40	99.61
455-1	35.64	3.32	26.19	0.12	–		0.91	0.55	–	31.25	–	97.99
455A-10	35.90	5.80	22.90	0.26	–	0.40	2.70	0.15	0.07	31.30	0.09	99.57
455A-8	31.00	5.10	28.70	–	–	0.40	1.80	–	–	32.70	–	99.70
456-15	29.88	4.30	30.40	0.29	–	0.71	1.40	0.12	0.54	32.10	–	99.74
456-5	38.40	6.10	23.10	–	–	0.55	0.80	–	–	30.20	0.28	99.43
456A-10a	31.49	3.75	29.36	0.18	–	–	1.63	0.13	–	33.13	0.22	99.89
456A-10b	31.50	2.60	29.80	–	–	–	2.90	–	–	32.80	–	99.60
617-1a	0.65	44.40	8.77	2.26	1.97	0.24	1.05	0.17	0.02	13.86	25.71	99.10
617A-3	28.35	4.30	30.20	0.71	–	1.45	–	–	–	31.99	1.50	98.50
617A-4-1	27.31	2.53	31.90	0.66	–	1.48	–	–	–	31.93	1.33	97.14
658-1	15.36	6.78	40.56	0.25	–	0.55	0.80	0.29	–	33.45	–	98.04
659-3	27.61	6.75	29.54	0.04	–	–	0.57	0.11	–	32.68	1.34	98.64
659-6	26.78	5.24	31.78	0.31	–	1.30	1.27	0.33	0.09	31.56	0.14	98.80
659-7	31.70	3.90	30.45	–	–	1.45	–	0.12	0.13	30.87	–	98.62
659-9	18.92	5.13	39.39	–	–	1.86	1.35	0.07	–	33.81	0.07	100.64
660-4a	19.00	5.11	40.48	–	–	1.54	1.02	0.05	0.04	33.64	–	100.88
660-5b	33.85	6.08	25.11	0.05	–	0.88	1.32	0.17	0.16	29.86	–	97.48
660As-5	17.41	7.52	40.71	0.73	–	–	–	0.12	–	33.13	–	99.62
660As-7	31.20	4.65	32.75	0.41	–	–	–	–	–	31.75	–	100.76
660Es-2b	22.12	8.87	38.08	–	–	–	0.95	0.15	–	31.13	0.50	101.80
660-1a	15.54	8.27	37.62	0.15	–	–	1.82	0.41	–	35.67	–	99.48
660-1b	23.29	7.61	32.19	0.25	–	1.39	1.98	0.19	–	31.37	–	98.27
660-1c	24.19	4.95	30.25	–	–	1.47	1.85	0.37	0.14	33.99	0.28	97.46

Table 2. *Cont.*

Erlichmanite	Os	Ir	Ru	Rh	Pt	Pd	Fe	Ni	Cu	S	As	total
609B-1*	57.02	13.96	0.92	0.12	–	–	1.02	0.07	–	23.54	1.77	98.42
373A-7a	56.40	13.40	1.40	–	0.09	–	–	–	–	25.70	0.23	97.22
456-9	50.23	6.83	11.65	–	–	0.91	1.26	0.09	–	26.82	0.48	98.26
456A-4a	47.43	3.33	16.75	0.15	–	–	0.39	0.11	–	29.77	0.08	98.01
660-10	30.49	21.13	14.67	–	–	0.68	1.26	0.11	–	25.74	4.85	98.93
660Bs-10	66.07	9.99	0.41	–	–	–	1.24	–	–	21.84	–	99.55
660Ds-6	38.67	5.09	26.12	0.06	–	–	0.89	0.04	–	29.10	–	99.97
660Es-1a	33.07	4.98	30.47	–	–	–	1.25	–	0.06	29.90	–	99.73

***** Samples from CHR-1.

Table 3. Electron microprobe compositions of PGM sulfides, sulfarsenides, alloys and bismuth-tellurides from Niquelândia.

	Os	Ir	Ru	Rh	Pt	Pd	Fe	Ni	Cu	S	As	Bi	Te	Sb	total
Malanite															
617A-5a-2	3.80	29.91	–	0.91	31.45	0.21	2.99	–	10.46	21.12	–	–	–	–	100.85
617A-5a-3	–	31.45	–	1.90	30.35	0.48	1.90	0.12	11.31	21.76	0.08	–	–	–	99.35
Irarsite															
617A-5b-4	–	53.50	0.62	4.58	0.79	1.28	2.40	–	0.70	11.11	25.22	–	–	–	100.20
660Es-2a	1.54	61.20	1.79	0.49	–	–	0.76	–	–	9.84	24.34	–	–	–	99.96
Os-Ir-Ru alloys															
373A-7b	76.61	21.55	0.33	–	–	–	–	–	–	0.19	–	–	–	–	98.68
455A-4	79.40	17.30	0.50	–	–	–	2.50	–	–	–	–	–	–	–	99.70
615E-5*	90.70	3.39	–	0.08	–	–	2.18	–	–	–	–	–	–	–	96.35
617-1b	55.29	22.70	17.22	0.57	3.74	–	0.82	–	–	–	–	–	–	–	100.34
660-9-3	49.43	43.67	0.30	–	–	–	5.17	0.75	–	–	–	–	–	–	99.32
661-1b	27.72	64.00	–	–	–	–	6.46	1.46	–	0.58	–	–	–	–	100.22
Pt-Fe Alloys															
55-1*	0.13	0.17	–	0.30	73.40	0.57	23.20	0.48	0.06	–	–	–	–	–	98.31
453-2	–	–	–	–	73.34	–	25.32	1.07	–	–	–	–	–	–	99.73
660-4b	–	–	–	0.32	76.25	–	16.31	6.22	–	–	–	–	–	–	99.10
661-1a	–	2.46	–	0.25	63.23	–	27.33	6.53	–	–	–	–	–	–	99.80
Pt- and Pd-bearing tellurides, bismuthides, and antimonides															
209I-10a*	–	–	–	–	0.60	35.87	0.65	2.53	–	–	–	37.13	16.48	6.70	99.96
209I-10b-1*	–	–	–	0.30	26.90	0.17	–	5.80	–	–	–	19.63	44.10	1.30	98.20
209I-10b-2*	–	12.76	–	–	33.76	1.31	0.76	2.90	–	–	–	5.62	11.25	27.43	95.79
209I-5*	–	13.95	–	0.43	28.10	–	1.27	2.09	–	–	–	1.60	7.00	45.45	99.89

***** Samples from CHR-1.

Figure 7. Ternary plot of Ru-Os-Ir sulfide and Pt-Fe alloy PGM associated with the chromitites of Niquel ândia.

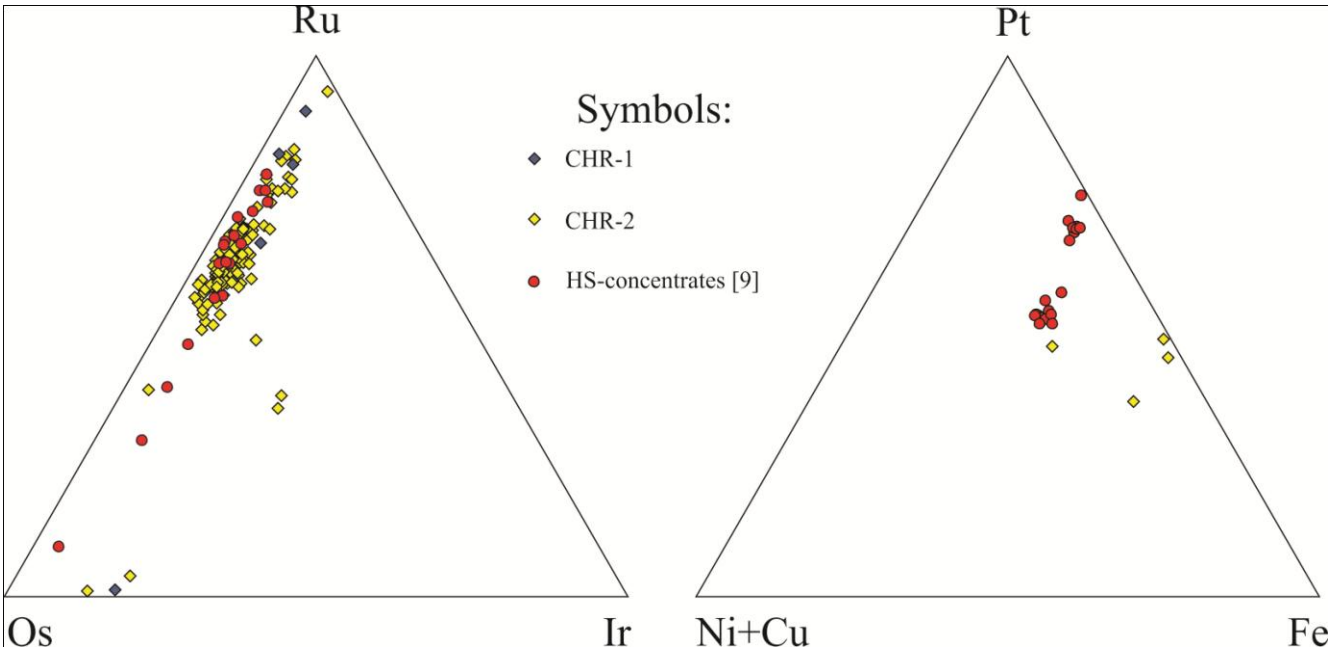

In the CHR-1 horizon, PGM have been found in both the chromitite and the adjacent dunite with different mineral assemblages in each case. The chromitite contains predominantly Ru-Os-Ir sulfides (mainly laurite) and alloys, mostly occurring included in fresh chromite. The PGM may occur as single phase or composite grains with Ni-sulfides (pentlandite, millerite) and silicate (clinopyroxene), or form minute spots within small blebs of pentlandite (Figure 8). The dunite contains Pt-Fe alloy included in orthopyroxene and laurite associated altered olivine (55-1, 55-3, Figure 9). Composite PGM of Pt-Pd-Bi-Te-Sb occur associated with partially-oxidized interstitial sulfide, or with the alteration rim of accessory chromite grains (Figure 9, 209I-10a, 209I-10b).

Sulfides of the laurite-erlichmanite series are the most common PGM in the CHR-2 chromitites. A few grains associated with phlogopite and amphibole respectively (Figure 10, 659-7 and 659-9) were found included in solid, low reflective chromite. Most of the other examples occur as anhedral to sub-euhedral crystals within the pitted high reflective chromite, sometimes associated with other PGM sulfides, alloys, or sulf-arsenides (Figure 11). In some case (Figure 12), sulfides of the laurite-erlichmanite series show a particular association with hematite, and rutile (456As-10a, 456As-10b), or are included in vermicular ilmenite at the boundary of large chromite grains (660-1). This type of laurite displays clear chemical zoning showing an irregular increase in Os towards the rim.

The study of concentrates obtained by hydroseparation (HS) has shown the widespread occurrence of various types of Pt-Fe alloys (with Pt_3Fe to Pt (Fe, Ni, Cu) stoichiometries) in chromitite samples from the CHR-2 horizon, characterized by a relatively coarse-grain size between 20 and 80 μm [9]. Such large grains were not encountered *in situ*, during the microscopic study of polished sections and the reason for the discrepancy is explained by the authors. Here we report new findings of Pt-Fe alloys after those described by [7] and give details of their unusual occurrence. Irregular grains of Pt-Fe alloys occur in secondary assemblages consisting of Fe-hydroxides and ilmenite associated with

kaolinite lamellae (Figure 13). Electron microprobe composition is consistent with a tetraferroplatinum-type stoichiometry PtFe, with abundant Ni and Cu substitution, whereas the isoferroplatinum-type compositions Pt_3Fe encountered in the concentrates have not been observed *in situ.*

Figure 8. Paragenetic assemblages of PGM associated with the CHR-1 chromitite (BSE images). 211C-1: Laurite + pentlandite + cpx composite inclusion in fresh chromite; 609B-1: Erlichmanite at the contact between chromite and serpentine (dark grey); 609B-2: Pentlandite + pyrrhotite + Ir-Os-(S) (white spots) composite inclusion in fresh chromite; 615A-1: Pentlandite + pyrrhotite + Ir-(S) (border white patch) + Os-(S) (horizontal white rod) composite inclusion in fresh chromite; 615A-2: Sub-euhedral laurite included in fresh chromite; 615F-6: Laurite + pentlandite composite inclusion in fresh chromite; 615E-5: Native Os included in fresh chromite; 609A-16: Euhedral laurite in the serpentine matrix of the CHR-1 chromitite; 609A-17: Pentlandite + Ir-sulfide in the alteration rim of a large chromite grain.

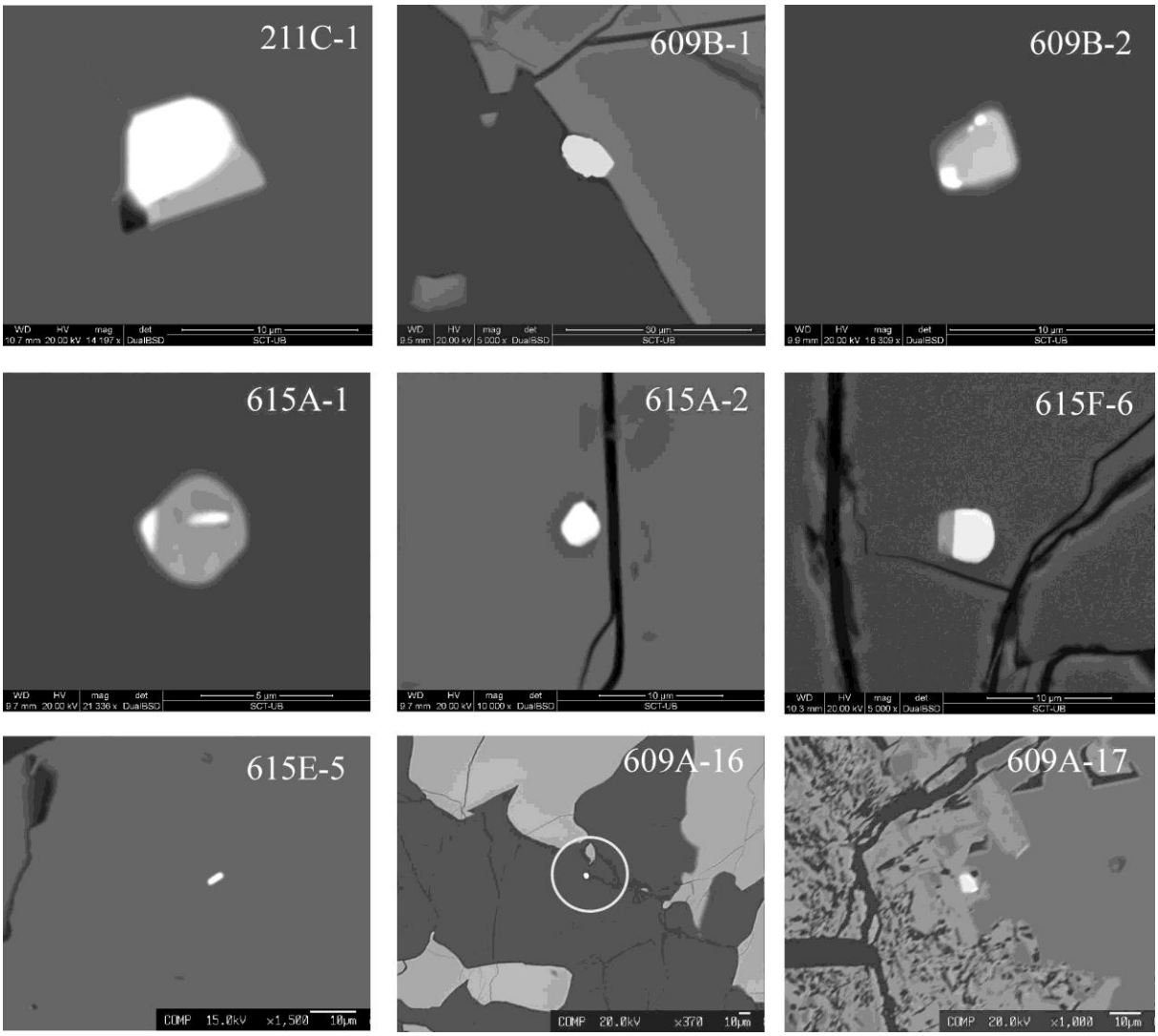

Figure 9. Paragenetic assemblages of PGM in the dunite adjacent to CHR-1 chromitite (BSE images). 55-1: Pt-Fe alloy included in opx; 55-2: Laurite in serpentine veins after olivine, in close proximity to pentlandite + native Cu after chalcopyrite (large grain); 209I-10a: Partially euhedral sobolevskite-kotulskite-sudburyite type PGM associated with pentlandite veined with magnetite, interstitial to serpentinized olivine and accessory chromite in dunite; 209I-10b: Composite grain of moncheite type and stumpflite type PGM attached to the rim of porous ferrian-chromite coating accessory chromite in dunite.

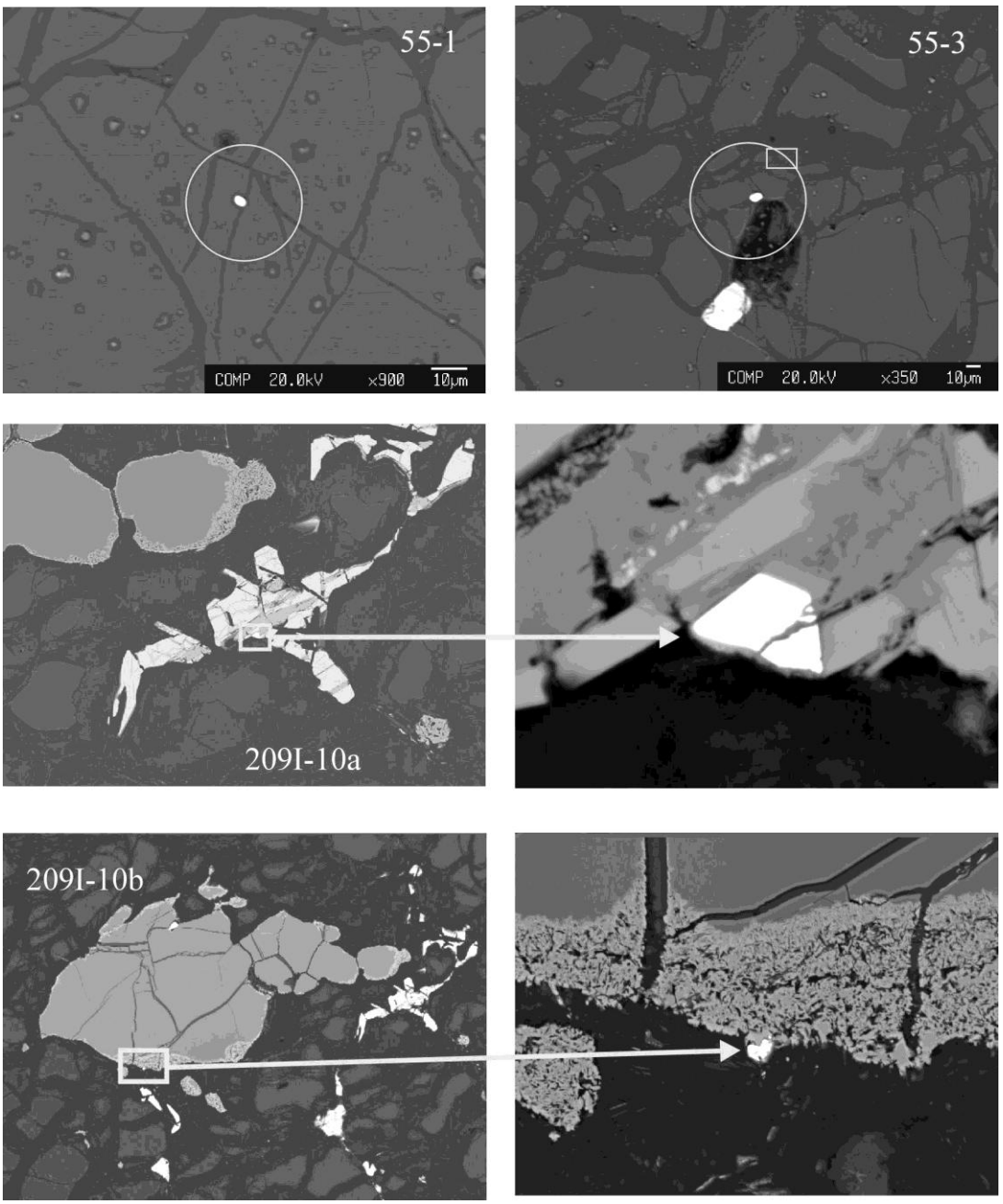

Figure 10. Paragenetic assemblages of Ru-Os-Ir PGM in the CHR-2 chromitite (BSE images). 660As-7: Euhedral grain of laurite with included pentlandite in chromite 2; 660As-5: Porous crystal of laurite + ferrianchromite located along crack in chromite 2; 660-2: Sub-euhedral erlichmanite + kaolinite included in chromite 2; 660-4a: Euhedral laurite + serpentine included in chromite; 659-7: Composite inclusion of laurite + phlogopite in chromite 1; 659-9: Composite inclusion of sub-euhedral erlichmanite + Ni-sulfide + amphibole in chromite 1; 660-5b: Sub-euhedral laurite + Fe-oxide + serpentine included in chromite 2; 659-6: Composite inclusion of laurite + Ir-sulfide + millerite + serpentine in chromite 2; 659-3: Composite inclusion of laurite + hematite + serpentine in chromite 2.

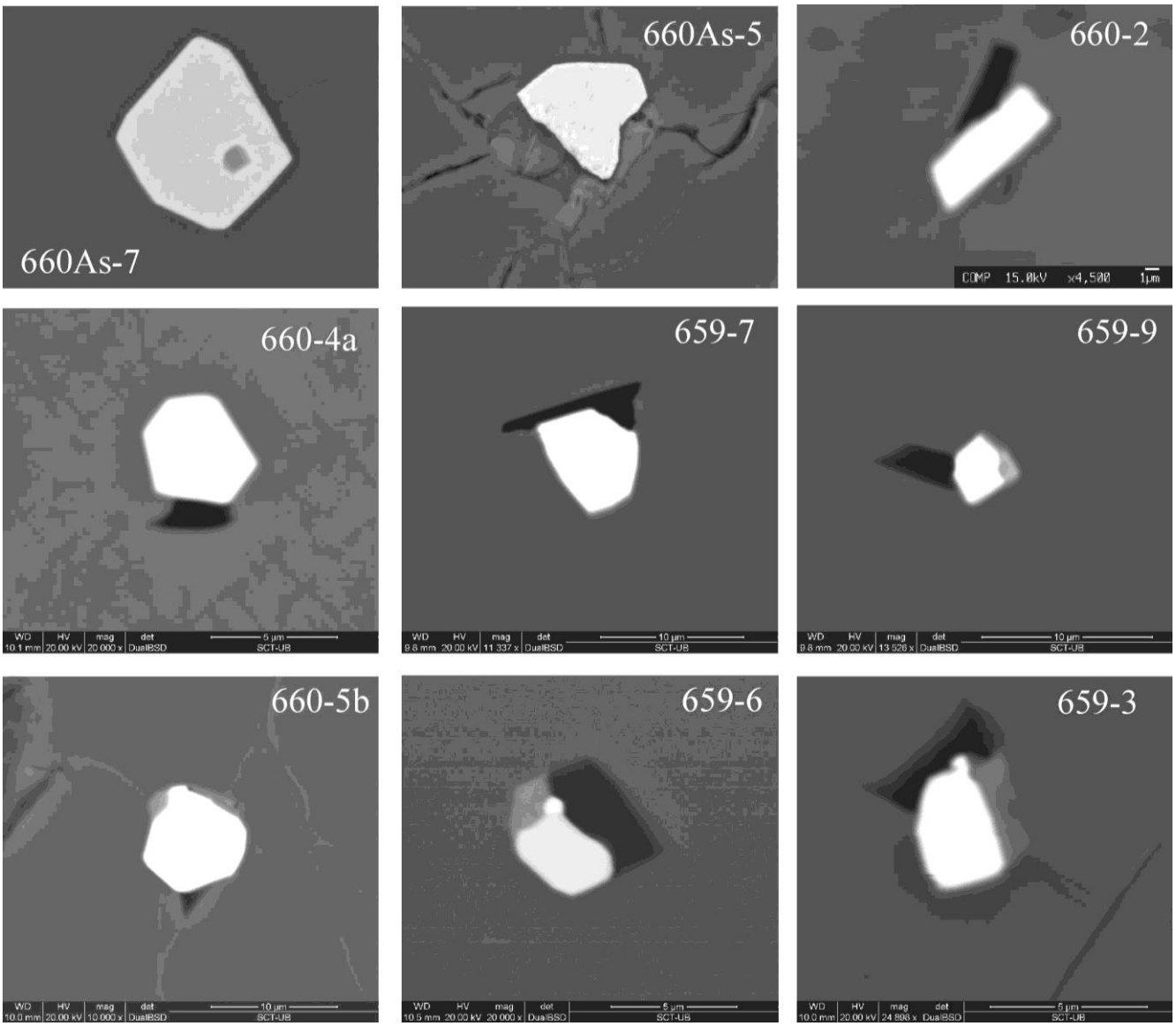

Figure 11. Paragenetic assemblages of Ru-Os-Ir PGM in the CHR-2 chromitite (BSE images). 373A-7: Euhedral composite grain of erlichmanite + iridosmine + pentlandite (dark crystal in the sulfide), included in chromite 2. 660Es-2: Partially altered composite grain of laurite + irarsite in fractured chromite 2. 617-1: Composite grain consisting of irarsite (low) + Os-alloy (middle) + laurite (upper) included in chromite 2.

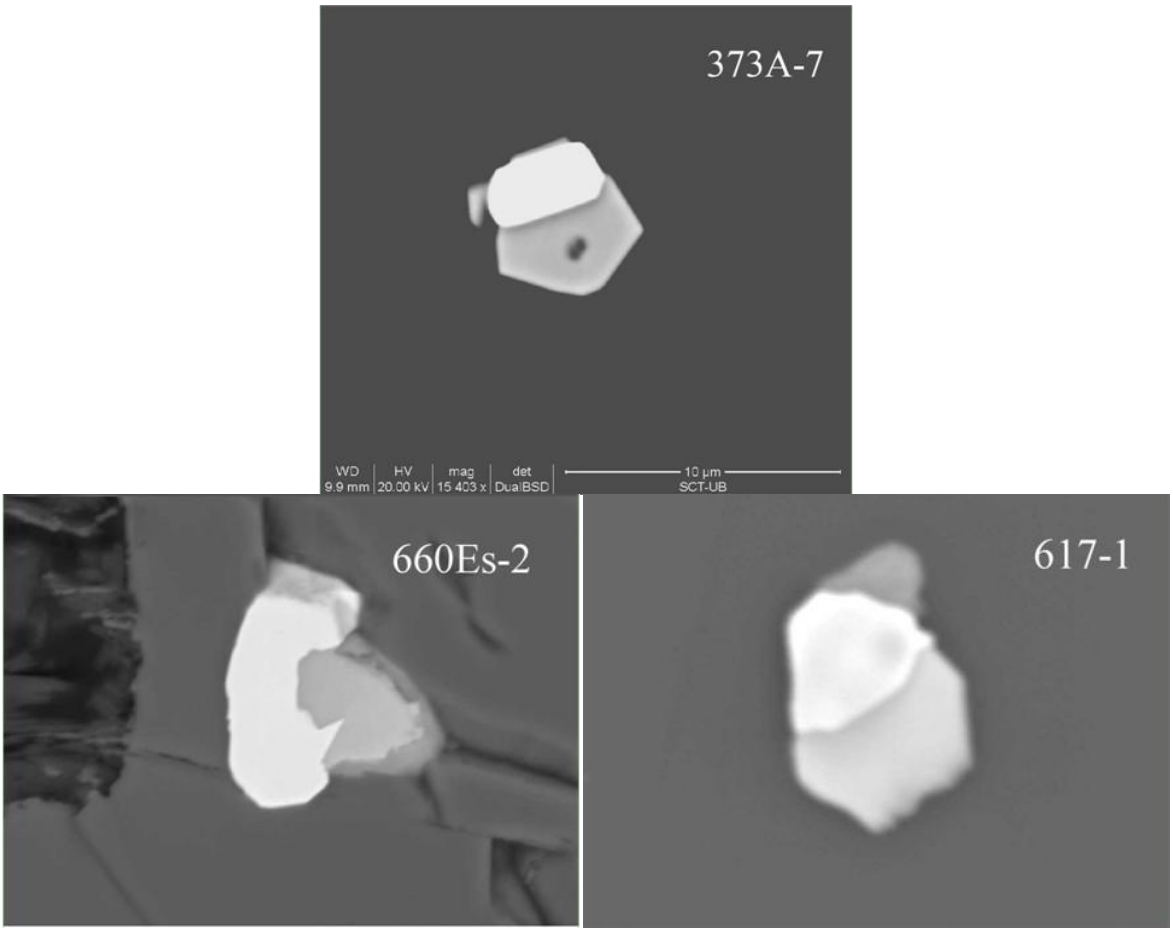

Figure 12. Paragenetic assemblages of Ru-Os-Ir PGM in the CHR-2 chromitite (BSE images). 660-1: Three laurite grains included in ilmenite; the laurite is strongly zoned showing Os-enriched rim. 456A-10a: Euhedral laurite associated with hematite included in chromite 1. 456A-10b: Sub-euhedral laurite associated with rutile in chromite 1.

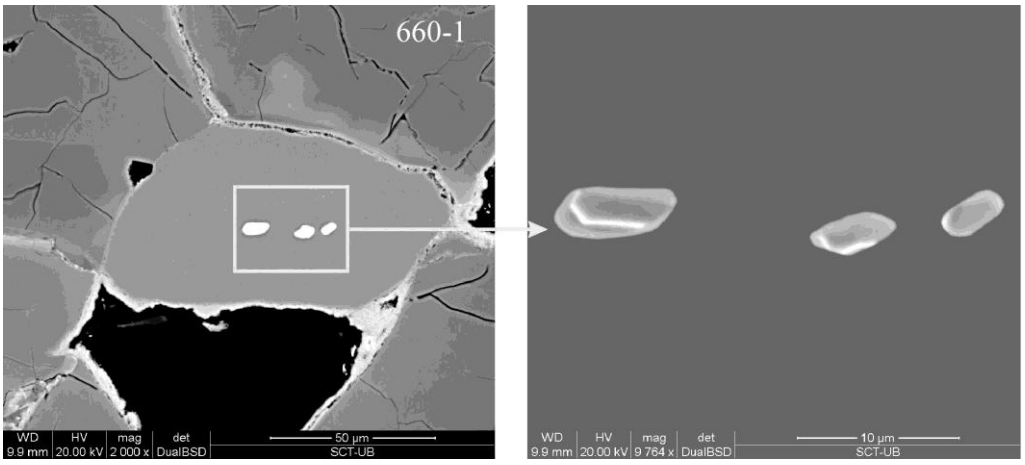

Figure 12. *Cont.*

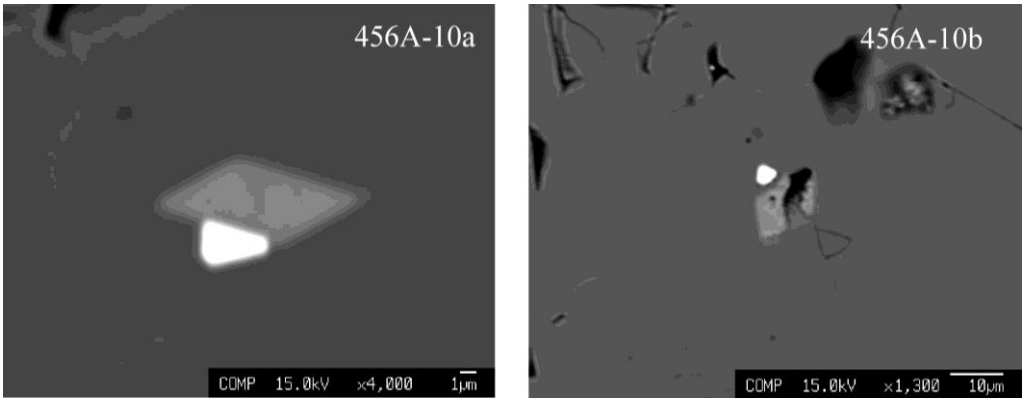

Figure 13. Paragenetic assemblages of Pt-Fe and Os-Ir alloys in the CHR-2 chromitite (BSE images). 373A-1: Large kaolinite lamella veined with Fe-hydroxides; a small grain of Pt-Fe alloy is located at the contact between kaolinite and a composite aggregate of Fe-hydroxide; an ilmenite crystal located along the fracture is visible in the NE corner of the large-field picture. 660-4: Pt-Fe alloy located in ilmenite at the contact with enclosing chromite 1; ilmenite occurs in a fracture with kaolinite and Fe-hydroxide; 661-1: Composite grain of Pt-Fe (light grey) and Os-Ir (white) alloys in Fe-hydroxide at the rim of a large kaolinite lamella; kaolinite is spotted and coated with botryoidal Fe-hydroxide; 660-9: Large grain of Os-Ir alloy at the rim of a large aggregate of Fe-hydroxide, located at the junction of frac tures in chromite 1.

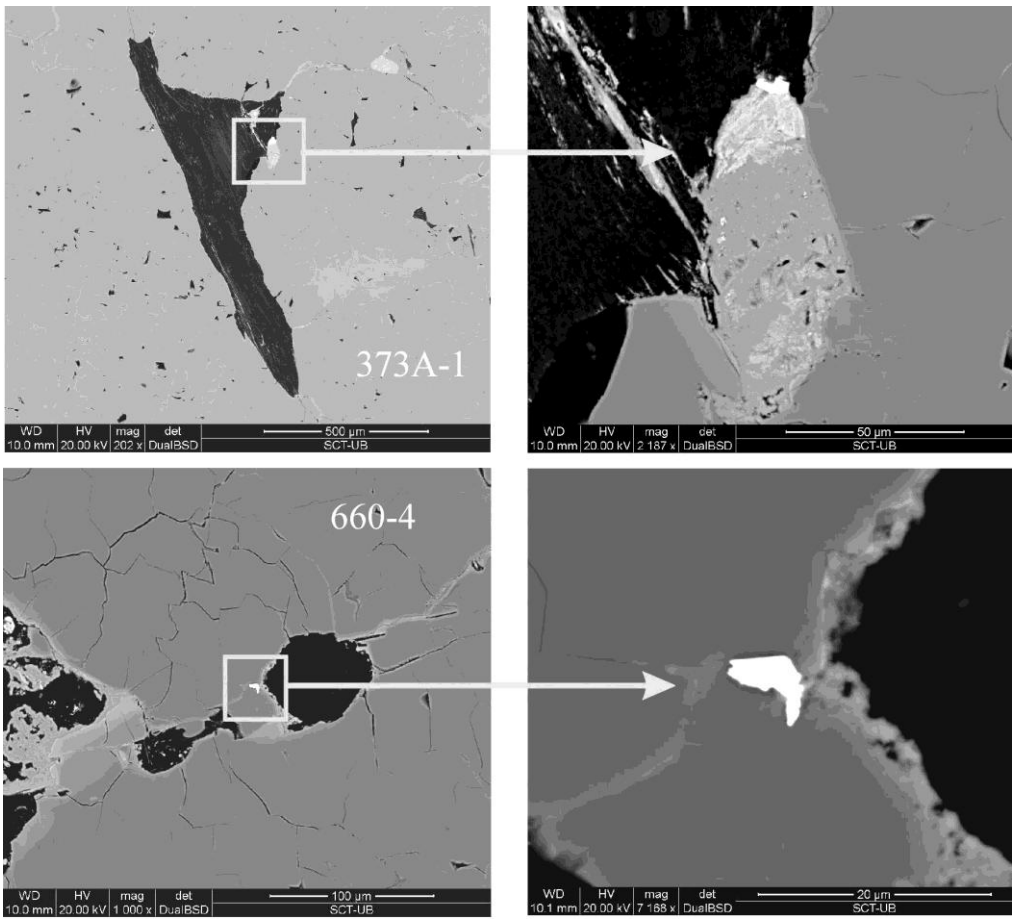

Figure 13. *Cont.*

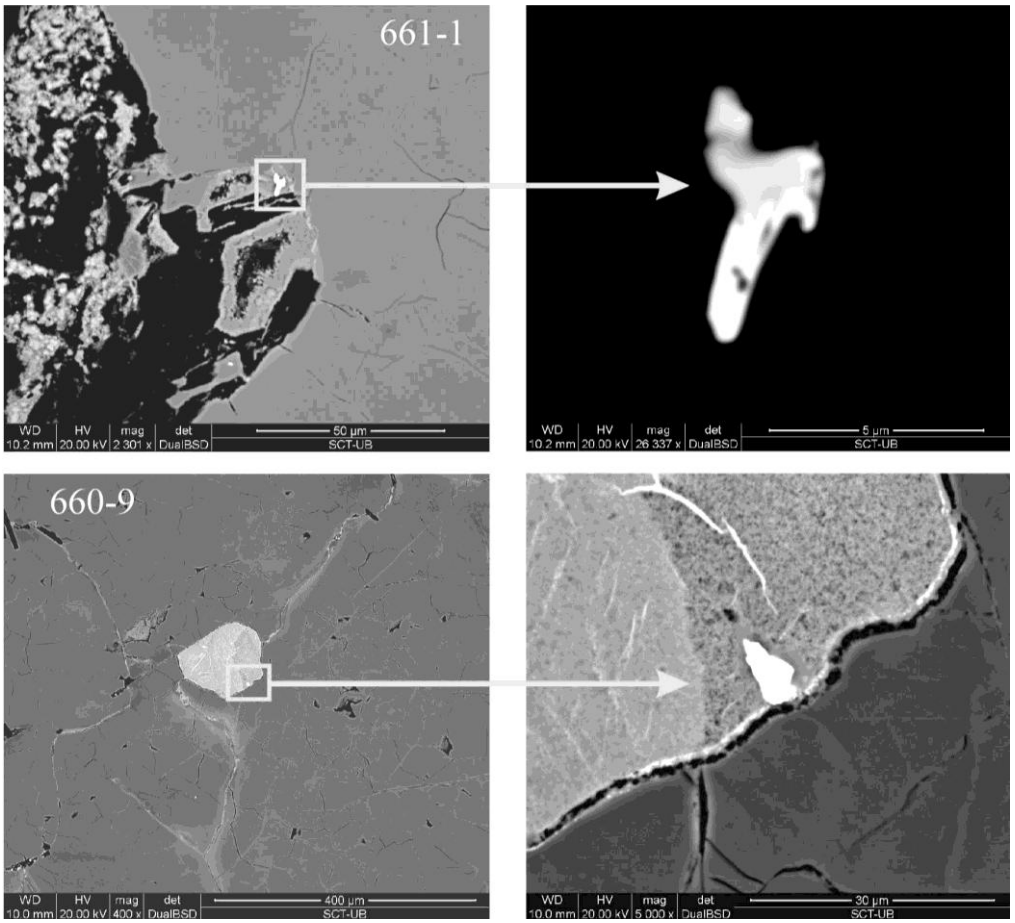

Similar to Pt-Fe alloys, other alloys of the Os-Ir-Ru type occur associated with secondary Fe-hydroxides, goethite and limonite (Figure 13, 661-1, 660-9). Finally, a large grain of Ru-oxide was encountered included in the pitted chromite of CHR-2. The grain consists of a Ru-O compound with minor Mn and Ni, just slightly more reflective than the surrounding chromite (see the optical and BSE images in Figure 14). The grain contains two bright lamellae of Ru-Os sulfide, possibly corresponding to laurite.

Figure 14. Paragenetic assemblages of PGE oxide in the CHR-2 chromitite (optical and BSE images). 660As-12: Large grain of Ru-Ir oxide with impurities of Mn, Ni and As; the internal white patches are relicts of Os-rich laurite.

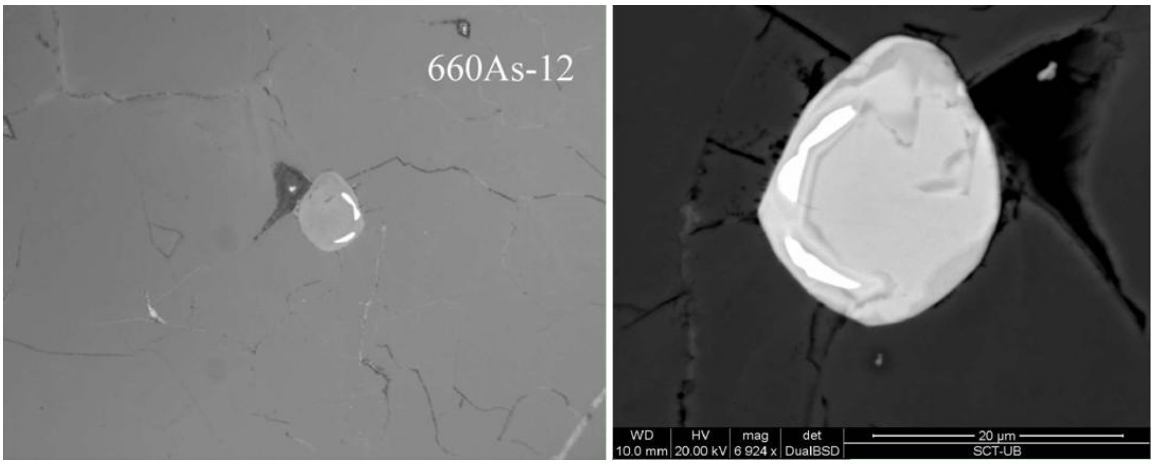

6. Constraints on the Origin of PGM in the Niquelândia Chromitites

As remarked by [7], chromitites of the Niquelândia layered intrusions contain two genetically different populations of PGM: (1) Primary PGM formed during fractionation of chromitite and dunite, at high-temperature; and (2) secondary PGM derived from *in-situ* alteration of primary PGM, or formed by mobilization of PGE during serpentinization and lateritic weathering.

Primary PGM in the chromitite-dunite assemblage of CHR-1 show a well defined order of crystallization. The early PGM are Ru-Os-Ir sulfides and alloys. They crystallized at high temperature and were mechanically trapped within growing chromite with small amounts of silicate and sulfide.

Despite the presence of sulfides in the assemblage, entrapment of these PGM is believed to have occurred before sulfur saturation of the melt [12]. During formation of the chromitite, Pt and Pd (with some IPGE) remained in the silicate melt. They precipitated later, collecting within the immiscible sulfide liquid segregated from the silicate magma after the main chromitite event. The sporadic occurrence of Pt-Fe alloys encapsulated in the orthopyroxene and laurite in serpentinized olivine suggests that some PGE were removed from the silicate melt at some stage of the dunite fractional crystallization when the melt was sulfur-undersaturated [7].

PGM inclusions were protected from serpentinization by the host chromite. Chromite is more resistant to alteration than silicates and sulfides. In contrast, PGM located in the rims of chromite grains or in the silicate gangue were exposed to alteration, and could have undergone secondary remobilization.

The origin of the PGM associated with the interstitial sulfides and ferrian-chromite in the CHR-1 dunite (Figure 9) is uncertain. They may represent relicts of primary Pt-Pd-Bi-Te-Sb minerals partially eroded by chemically aggressive solutions, during serpentinization, or even PGM precipitated from the solution itself, as reported for similar Pt-Pd phases in the altered silicate matrix of the Campo Formoso chromitites [13]. In one case, the euhedral shape of the partially eroded Pt-Bi-Te grain associated with the sulfide (Figure 9, 209I-10b) would suggest that it is a relict of a primary phase surviving alteration.

In general, it is difficult to identify the primary or secondary origin of the Os-Ir-Ru PGM in the CHR-2 chromitite. However, based on their texture and morphology, most of the Ru-Os-Ir sulfides, sulfarsenides and alloys included in the CHR-2 chromitite represent primary phases that survived alteration of the enclosing chromite, due to their higher chemical stability compared with the chromite. Notably, if the Ir-Os sulfarsenides represent primary phases we have to admit an increase of the As/S activity ratio in the CHR-2 chromite-forming system compared with CHR-1 that could have taken place in response to As-S fractionation due to differentiation. This question is unresolved. Some Ru-Os-Ir sulfides, however, display evidence of chemical corrosion (660As-5, Figure 10), others are intimately associated with secondary silicates: serpentine (659-3, 659-6, 660-5b, 660-4a, Figure 10) or kaolinite (660-2, Figure 10) and therefore, their primary or secondary origin is unclear. The laurite inclusions in vermicular ilmenite (660-1, Figure 12) would appear to have formed during precipitation of ilmenite, a process that could have occurred at relatively low-temperature as a result of Ti loss during chromite alteration. The close association of the tetraferroplatinum type alloys with kaolinite plus Fe-hydroxides is a clear indication that the Pt-PGM were deposited during low temperature alteration. The primary isoferroplatinum type alloys recovered from HS concentrates, might represent the primary source for Pt remobilization. The Pt is re-deposited at the interface between kaolinite and Fe hydroxides, possibly representing a local redox micro-boundary necessary to trigger Pt precipitation

(Bowles, 1986). The evidence that PGE were mobilized during the lateritization process is provided by the finding of PGE oxides associated with altered chromitite. The internal texture of the PGM in Figure 14 clearly indicates that the Ru-oxide is derived from alteration of a laurite precursor whose relict is still preserved. As shown in other occurrences elsewhere [14], alteration of laurite involves removing of S and Os, which are replaced by O and small amounts of base metals (Fe, Mn, Ni).

7. Conclusions

The PGM assemblages observed in the Niquelândia complex, indicate primary deposition of the IPGE during accumulation of chromite, and precipitation of the PPGE by segregation of an immiscible sulfide liquid, following the chromitite event. The PGM are only weakly affected by late serpentinization, especially those associated with interstitial silicates and sulfides in dunite. Conversely, secondary mobilization and redistribution of PGE appears to be more extensive during laterite weathering of the chromitites and their country rock. Primary Ru-Os sulfides included in the chromite become unstable under the action of lateritic solution, and are oxidized or re-crystallize developing conspicuous chemical zoning. Paragenetic observation suggests that Pt is particularly mobile under this type of weathering as proposed for other altered igneous complexes [15]. In particular, it re-precipitates inside the altered chromitite possibly as a result of redox variations on the microscopic scale. These Pt-enriched altered chromitites represent a potential lode deposit for the generation of Pt-placers which may be present somewhere inside the extensive laterite cover of the Niquelândia complex.

Acknowledgments

The authors wish to thank Maria Economou-Eliopoulos and the anonymous reviewers for their comments and suggestions that have improved the manuscript. The University Centrum for Applied Geosciences (UCAG) is thanked for the access to the E. F. Stumpfl electron microprobe laboratory. This research has been partially financed by the Spanish grants CGL2009-10924 and CGL2012-36263.

References

1. Fleischer, R.; Routhier, P. Quelques grands themes de la geologie du Bresil: Miscellanes geologiques et metallogeniques sur le Planalto. *Sci. Terre* **1970**, *15*, 45–102.
2. Pimentel, M.M.; Ferreira Filho, C.F.; Armstrong, R.A. SHRIMP U-Pb and Sm-Nd ages of the Niquelândia layered complex: Meso-(1.25 Ga) and Neoproterozoic (0.79 Ga) extensional events in central Brazil. *Precamb. Res.* **2004**, *132*, 133–153.
3. Ferreira Filho, C.F.; Pimentel, M.M.; Araujo, S.M.; Laux, J.H. Layered intrusions and volcanic sequences in central Brazil: Geological and geochronological constraints for Mesoproterozoic (1.25 Ga) and Neoproterozoic (0.79 Ga) igneous associations. *Precamb. Res.* **2010**, *183*, 617–634.
4. Ferreira Filho, C.F.; Pimentel, M.M. Sm-Nd isotope systematics and REE data for leucitroctolites and their amphibolitized equivalents of the Niquelândia complex upper layered series, central Brazil: Further constraints for the timing of magmatism and high-grade metamorphism. *J. South Am. Earth Sci.* **2000**, *13*, 647–659.

5. Barros de Oliveira, S.M.; Trescases, J.J.; Melfi, A.J. Lateritic nickel deposits of Brazil. *Mineral. Deposita* **1992**, *27*, 137–146.
6. White, R.W.; Motta, J.; Arraujo, V.A. Platiniferous chromitite in the Tocantins complex, Niquelandia, Goias, Brazil. In *Geological Survey Research 1971*; U.S. Geological Survey, Ed.; U.S. Government Printing Office: Washington, DC, USA, 1971; pp. 26–33.
7. Ferrario, A.; Garuti, G. Platinum-group minerals in chromite-rich horizons of the Niquelândia Complex (Central Goias, Brazil). In *Geo-Platinum 87*; Prichard, H.M., Potts, P.J., Bowels, J.F.W., Cribb, S.J., Eds.; Elsevier Applied Sciences: London, UK, 1988; pp. 261–272.
8. Miliotti, C.A.; Stumpfl, E.F. Platinum-group mineral inclusions, textures and distrbution in the chromitites of the Niquelândia Complex, Brazil. In *Brazilian Meeting on Platinum-Group Element*: *Extended Abstract Volume*; Jost, H., Macedo, D., Eds.; Brazilian Geological Society: Brasilia, Brazil, 1993; pp. 33–35.
9. Rudashevsky, N.S.; Garuti, G.; Andersen, J.C.Ø.; Krester, Y.L.; Rudashevsky, V.N.; Zaccarini, F. Separation of accessory minerals from rocks and ores by hydroseparation (HS) technology: Method and application to CHR-2 chromitite, Niquelândia intrusion, Brazil. *Trans. Inst. Min. Metall. B* **2002**, *111*, 87–94.
10. Garuti, G.; Rivalenti, G.; Girardi, V.A.V.; Brigo, L.; Fornoni Candia, M.A. Metalogenese dos sulfetos do complexo de Niquelandia, Goias (Brazil). In *Boletim n.1, Resumos e Breves Comunicaçoes*, Proceeding of XXXIV Congresso Brasileiro de Geologia, Goiania, Brazil, 12–19 October 1986.
11. Thompson, J.F.H.; Barnes, S.J.; Duke, J.M. The distribution of nickel and iron between olivine and magmatic sulfides in some natural assemblages. *Can. Mineral.* **1984**, *22*, 55–66.
12. Brenan, J.M.; Andrews, D. High-temperatures stability of laurite and Ru-Os-Ir alloy and their role in PGE fractionation in mafic magmas. *Can. Mineral*. **2001**, *39*, 341–360.
13. Garuti, G.; Proenza, J.A.; Zaccarini, F. Distribution and mineralogy of platinum-group elements in altered chromitites of the Campo Formoso layered intrusion (Bahia State, Brazil): Control by magmatic and hydrothermal processes. *Mineral. Petrol.* **2007**, *86*, 159–188.
14. Garuti, G.; Zaccarini, F. *In situ* alteration of platinum-group minerals at low temperature: Evidence from serpentinized and weathered chromitite of the Vourinos Complex, Greece. *Can. Mineral.* **1998**, *35*, 611-626.
15. Bowles, J.F.W. The development of platinum-group minerals in laterites. *Econ. Geol.* **1986**, *81*, 1278–1285.

© 2012 by the authors; licensee MDPI, Basel, Switzerland. This article is an open access article distributed under the terms and conditions of the Creative Commons Attribution license (http://creativecommons.org/licenses/by/3.0/).